Int. J. Electrochem. Sci., 16 **(2021)** Article ID: 210818, doi: 10.20964/2021.08.01

International Journal of
ELECTROCHEMICAL
SCIENCE
www.electrochemsci.org

Oxygen Reduction on Glassy Carbon-Supported PdAu Nanoparticles in Perchloric Acid Solution

Jelena Golubović[1], *Irina Srejić*[2], *Svetlana Štrbac*[1,*]

[1] ICTM-Department of Electrochemistry, University of Belgrade, Njegoševa 12, 11000 Belgrade, Serbia
[2] INS Vinča, Laboratory of Atomic Physics, University of Belgrade, Mike Alasa 12-14, 11001 Belgrade, Serbia
[*]E-mail: sstrbac@tmf.bg.ac.rs

Received: 6 April 2021 / *Accepted:* 27 May 2021 / *Published:* 30 June 2021

PdAu/GC nanoparticles obtained by the electrochemical deposition of gold followed by the spontaneous palladium deposition show a remarkable catalytic activity for the oxygen reduction reaction (ORR) in perchloric acid solution. AFM images reveal the size, shape, and coverage of the GC electrode with Au and PdAu nanoislands. Au/GC electrode with the full GC coverage by the deposited gold islands and activated by potential cycling shows the highest ORR activity. The initial potential for ORR shifts positively for 200 mV compared to polycrystalline gold. With the addition of palladium, the activity for ORR enhances significantly. For the most active PdAu/GC electrode, the initial potential shifts positively for another 250 mV, which coincides with polycrystalline palladium.

Keywords: Gold, palladium, glassy carbon, oxygen reduction, acid solution

1. INTRODUCTION

Oxygen reduction reaction (ORR) is one of the most common cathodic reactions in electrocatalysis. It has been studied systematically in acid solution on different gold electrodes including polycrystalline gold [1] and various gold single crystals [2]. Although gold shows much lower activity for ORR in acid than in alkaline solutions [3], it can generally be improved by the electrochemical activation [4-6]. Numerous studies have shown that the activity of carbon-supported gold nanoparticles, Au/GC, equals or even surpasses that of Au(poly) [7-15]. These studies involved the effect of size, number, and preferential orientation of Au nanoparticles (NPs). Besides, the Au/GC surface activation by potential cycling is also reported [4,16,17]. Such electrochemical activation is a consequence of the increase of surface roughness and the number of active surface sites. In contrast to the ORR on Au single crystals in alkaline solution, where the mechanism is strongly dependent on the surface orientation, in

acid solution, ORR proceeds as a $2e^-$ process on all Au single crystal faces [2]. Therefore, the Au/GC activation affects the positive shift of the potential rather than the current density.

The catalytic activity in acid solution can be improved significantly by modification with palladium of both Au single crystals [18] and polycrystalline gold [19,20]. Multilayer gold nanoclusters modified by electrodeposited Pd show enhanced electrocatalytic activity for ORR [21]. We have shown in our previous study that the mechanism for ORR in perchloric acid solution changes from $2e^-$-reduction on bare gold to $4e^-$-reduction on Pd/Au(poly), the fraction of which increases with the increase of Pd coverage [20]. Such an increase of activity for ORR with the addition of palladium on glassy carbon-supported Au nanostructures was also reported [22-24]. Besides, on carbon-supported porous Pd layer-coated Au nanoparticles (AuPd/C/GC) with Au/Pd weight % ratio of 0.6, ORR proceeds as a $4e^-$-process in sulfuric acid solution, exceeding the activity of both Pt(poly) and Pt/GC [22]. The cause of such high ORR activity is the porosity of the Pd shell layer on the Au core. Among different carbon-supported $Pd_{1-x}Au_x$ bimetallic nanowires, the Pd_9Au display superior electrocatalytic performance for ORR [23]. On the other hand, among different carbon-supported porous Pd shell coated Au nanochain networks, the $Au_{0.8}Pd_{0.2}$ has shown the highest activity for ORR in perchloric acid solution [24]. In a recent critical review [25], various synthesis methods for Pd-metal (including Pd-Au) alloys are listed and discussed. Besides, the activity towards ORR of supported different Pd-Au alloy catalysts are summarized and compared.

In this work, gold will be electrochemically deposited on glassy carbon support to form Au/GC with different coverage of gold, and then activated by potential cycling. Such Au/GC electrodes will additionally be modified with Pd using a spontaneous deposition method. The resulting PdAu/GC electrodes will be characterized *ex situ* using Atomic Force Microscopy (AFM) technique. The electrochemical characterization will be performed by Cyclic Voltammetry (CV) in deaerated perchloric acid solution. The activity of the obtained Au/GC and PdAu/GC electrodes for ORR will be examined by Linear Sweep Voltammetry (LSV) in oxygen saturated perchloric acid solution using a Rotating-Disc Electrode (RDE) technique.

2. EXPERIMENTAL

2.1. Preparation of Au/GC and PdAu/GC electrodes

Support electrodes were glassy carbon discs (5 mm in diameter, Alfa Aesar) for *ex-situ* surface characterization and mounted in a Teflon holder for electrochemical measurements. Before each deposition of gold, the GC support electrode was cycled ten times in deaerated 0.1 M $HClO_4$ solution in the potential range from - 0.25 V to 0.95 V.

The working Au/GC electrodes were prepared by the electrochemical deposition of gold, as described in our previous work [26]. Briefly, the Au nanoparticles were electro-deposited on GC by holding the electrode potential at - 0.3 V for various duration in 10^{-4} M $HAuCl_4$ + 0.5 M H_2SO_4 solution. For 5, 10, and 30 minutes gold deposition, the electrodes obtained are denoted as 5minAu/GC, 10minAu/GC, and 30minAu/GC, respectively. The surface was activated electrochemically by the

cycling potential in the range from - 0.20 V to 1.35 V. The working PdAu/GC electrodes were prepared by spontaneous palladium deposition on previously prepared Au/GC electrodes by their immersion in 1 mM $PdSO_4 \cdot 2H_2O$ + 0.05 M H_2SO_4 solution at the open circuit potential. Results presented in this work are for Pd deposition on 30minAu/GC electrode due to its highest activity for ORR (see below). For the chosen palladium deposition times of 3 and 30 minutes, the obtained electrodes are denoted as 3minPd30minAu/GC and 30minPd30minAu/GC, respectively.

2.2. AFM imaging of the electrode surfaces

AFM imaging of as-prepared Au/GC and PdAu/GC electrodes was performed using Multimode Quadrex SPM (Veeco Instruments, Inc.) with a silicon probe (Tip-Vista probe, tip radius <10 nm) in a tapping mode. Both height and phase images were both taken simultaneously during scanning over the same surface area. While height images provide information on surface topography, the phase images allow determining the coverage of GC with the Au or PdAu islands. The degree of chemical change of GC due to modification with Au and Pd is determined based on the phase images. AFM images were analyzed using the WSxM program [27].

2.3. Electrochemical measurements

The electrochemical characterizations of bare GC, Au/GC, and PdAu/GC working electrodes were performed using Pine Instruments Potentiostat in a three-electrode cell, with Pt wire as a counter and Ag/AgCl (3 M KCl) as a reference electrode. The measurements were conducted at room temperature in deaerated 0.1 M $HClO_4$ solution using Cyclic Voltammetry. Linear Sweep Voltammetry and Rotating Disc Electrode method were used to investigate the electrocatalytic properties of obtained surfaces for the oxygen reduction reaction in the same working solution but saturated with oxygen. Polarization curves were recorded in the cathodic direction in the potential range from 0.5 V to -0.3 V for Au/GC and from 0.7 V to -0.2 V for PdAu/GC electrodes while rotating at 1600 rpm. In the latter case, before each measurement, the electrodes were held for 15 minutes at the potential of - 0.05 V in 0.1 M $HClO_4$ solution to reduce the deposited palladium oxide into a metallic state. All cyclic voltammograms are recorded at a scan rate of 50 mV/s. The current density values are given relative to the geometric surface area of the working electrodes.

2.4. Chemicals

Supra pure $HClO_4$ (Merck), $HAuCl_4$(aq) (MaTeck), $PdSO_4 \cdot 2H_2O$ (Alfa Aesar), and Milli-pure water were used to prepare the working and depositing solutions. For CV measurements, the electrolytes were deaerated by high-purity nitrogen (Messer, 99.999%), while ORR measurements were performed in the electrolyte saturated by high-purity oxygen (Messer, 99.9995%).

3. RESULTS AND DISCUSSION

3.1. AFM imaging of Au/GC and PdAu/GC surfaces

Au/GC electrode obtained after electrochemical deposition of Au by holding the potential at -0.3 V for 30 min, shows the highest activity for ORR among all other Au/GC electrodes, as shown below. Also, when followed by 30 min spontaneous Pd deposition, the resulting PdAu/GC electrode shows the highest ORR activity. Figure 1 shows AFM images taken simultaneously in the height and phase mode, of these representative 30minAu/GC and 30minPd30minAu/GC electrode surfaces. Surface topography image of 30minAu/GC, Figure 1a, reveals that Au deposit consists of large islands with smooth edges distributed all over the GC substrate. The estimated average height of the deposited islands is 8.5 nm (approx. 35 Au monolayer), while the average surface roughness is 1.9. Phase AFM image, Figure 1b, shows that the coverage of the GC surface with the deposited Au islands is (93 ± 2) %. Cross-section analysis of the phase image, Figure 1c, shows that the lateral size of the Au islands ranged from 10-50 nm. The phase distribution, Figure 1d, indicates that the Au/GC surface consists of two chemically different components.

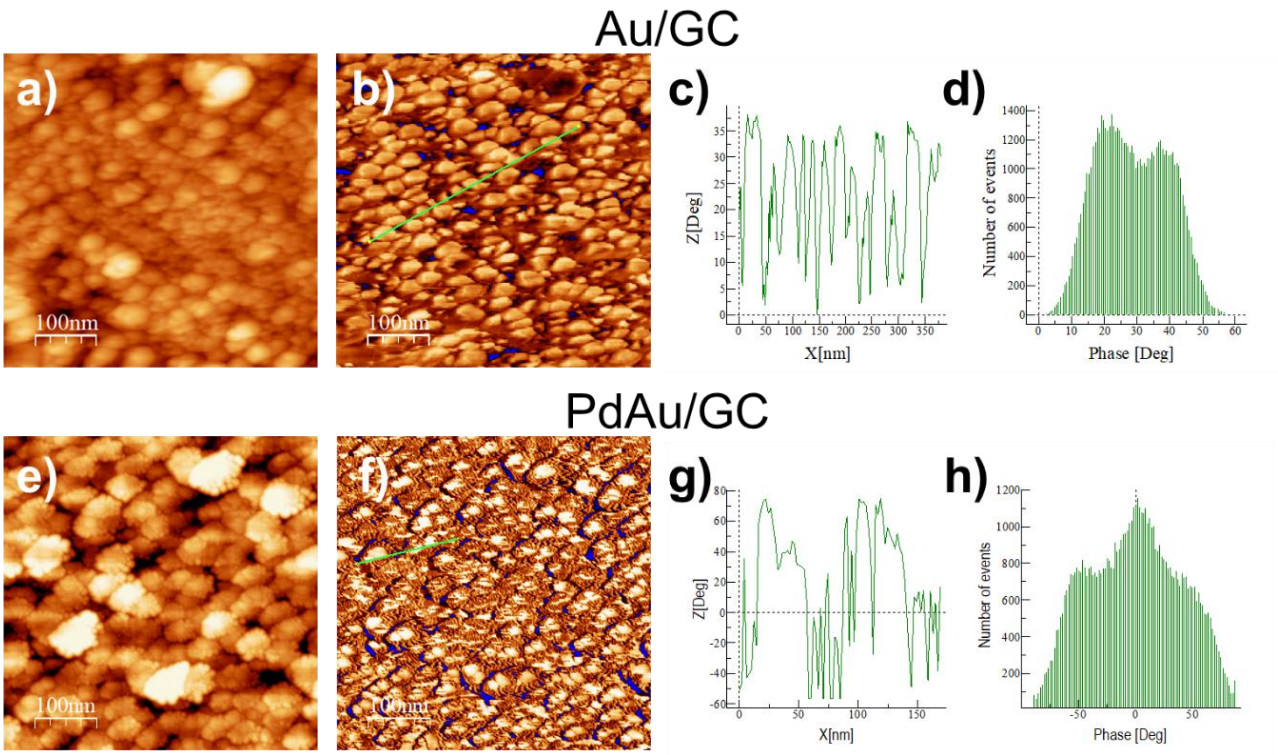

Figure 1. AFM images showing: a) surface topography of Au/GC (z-range = 20 nm; b) corresponding phase image (z-range = 62.2 Deg); c) cross-section along the line given in the phase image; d) phase-lag distribution; e) surface topography of PdAu/GC (z-range = 20 nm); f) corresponding phase image (z-range = 77.2 Deg); g) cross-section along the line given in the phase image; h) phase-lag distribution.

Surface topography image of 30minPd30minAu/GC, Figure 1e, reveals that PdAu islands are large with uneven and cracked edges. The average island height of 7.4 nm is lower concerning the individual Au islands, which indicates the preferred deposition of Pd on their edges. The average

30minPd30minAu/GC surface roughness is 2.9, which is higher concerning the 30minAu/GC. From a corresponding phase AFM image, Figure 1f, the estimated coverage is (98 ± 2) %. Cross-section along the line indicated in the phase image, Figure 1g, shows that the lateral size of the deposited PdAu islands ranged from 25-75 nm. The phase distribution, Figure 1h, indicates that the PdAu/GC surface consists of three chemically different components.

3.2. Electrochemical behavior of Au/GC electrodes

Figure 2 shows the CVs of different Au/GC electrodes recorded in 0.1 M $HClO_4$ solution. For comparison, it also shows the CVs of bare GC and polycrystalline gold, Au(poly), electrodes. The activation of Au/GC electrodes was performed by continuous cycling in the potential range from - 0.2 V to 1.35 V. Figure 2a shows the first and the 30th cycle for the electrode obtained after 30 minutes Au electrodeposition on GC substrate (denoted as 30minAu/GC). The first CV shows a wider double-layer region, the anodic oxidation, and cathodic reduction of electrodeposited gold. Apart from the appearance of a small shoulder at ca. 1.04 V, the characteristic CV features for the oxidation of gold in perchloric acid solution are missing. Namely, the missing peak is associated with the formation of AuOH on the gold surface free of adsorbed anions [28, 29], and its intensity correlates with the existence of surface defects involving the presence of steps, their density and orientation [30,31]. This peak becomes much more pronounced after 30 cycles, and the shape of the oxidation part of the CV obtained in the 30th cycle becomes very similar to the bare Au(poly) electrode. Those changes in the intensity of oxidation peaks could be related to the increase in the number of surface defects caused by continuous cycling of the electrode. During cycling, a partial disintegration and rearrangement of gold nanoparticles occurs, which has also been observed by the other authors [32-34].

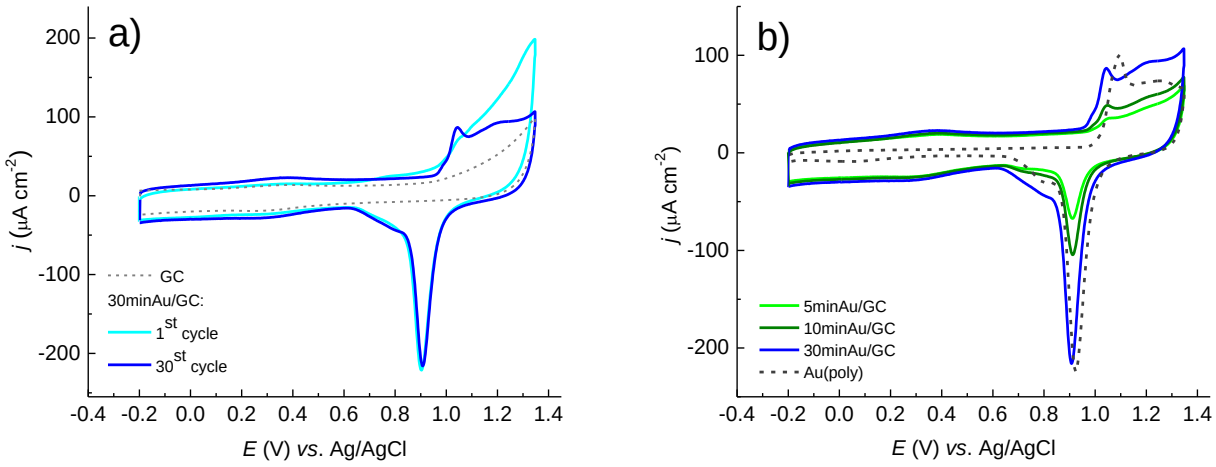

Figure 2. Cyclic voltammograms of Au/GC electrodes recorded in deaerated 0.1 M $HClO_4$ solution showing: a) the electrochemical activation of 30minAu/GC electrode with cycling; b) the difference in CV features of the activated Au/GC electrodes obtained for various deposition times. CVs of GC and Au(poly) are presented for comparison. The scan rate was 50 mV/s.

Figure 2b shows CVs of bare Au(poly) and different Au/GC electrodes obtained after Au was electrodeposited for 5, 10, and 30 min on GC and activated by continuous cycling. At lower potentials, the double layer on CVs for Au/GC electrodes are wider than the one for bare Au(poly), which indicates the influence of GC substrate. At higher potentials, the obtained anodic and cathodic peaks on Au/GC surfaces that originate from the oxidation and reduction of the deposited gold are following the characteristic peaks of the Au(poly) electrode. The oxidation process at Au/GC electrodes begins at the potential of 0.95 V, while the main reduction peak occurs at ca. 0.91 V. The CV for 30minAu/GC electrode shows the most pronounced oxidation/reduction peaks. The coverage of the GC electrodes with the deposited Au islands can be calculated from the ratio between the amount of charge passed during the reduction of gold oxide on Au/GC and oxide monolayer on bare Au(poly) electrode (400 $\mu C/cm^2$). The obtained coverage values are 28.0%, 45.9%, and 96.9% for 5, 10, and 30 minutes of Au electrodeposition on GC electrode, respectively.

Figure 3 shows polarization curves, obtained using Linear Sweep Voltammetry (LSV curves), for the oxygen reduction reaction on bare GC, Au(poly), and different Au/GC electrodes in oxygen saturated 0.1 M $HClO_4$ solution. For comparison, only LSV curves recorded at 1600 rpm are presented.

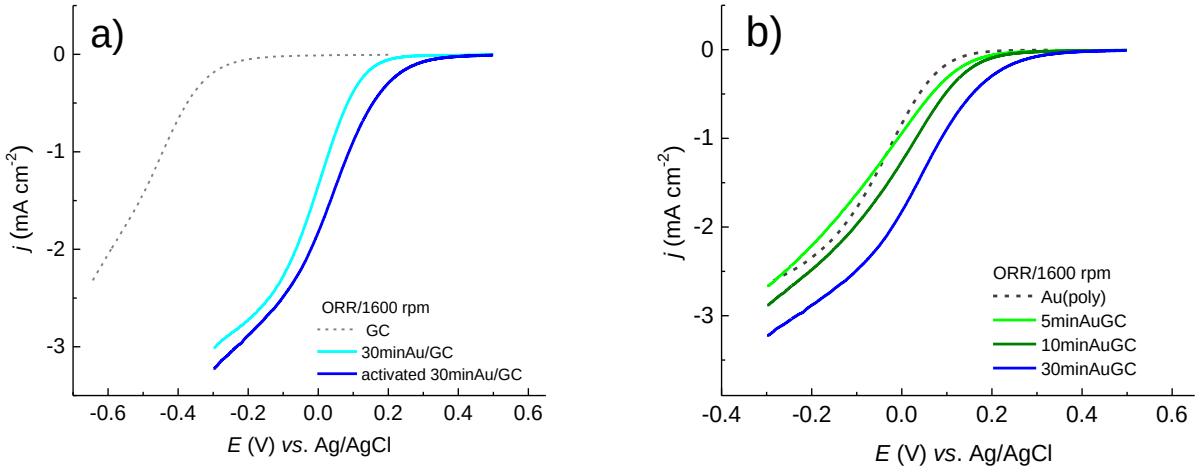

Figure 3. Polarization curves for ORR recorded at 1600 rpm in 0.1 M $HClO_4$ solution saturated with oxygen: a) freshly prepared and electrochemically activated 30minAu/GC electrodes and bare GC; b) different activated Au/GC electrodes and Au(poly). The scan rate was 50 mV/s.

The polarization curves for ORR on bare GC and the 30minAu/GC electrode recorded immediately after Au deposition and after the activation of the electrode by continuous cycling are shown in Figure 3a. GC electrode alone is the bad catalyst for oxygen reduction since the reaction occurs at high overpotentials. When modified with gold, the resulting Au/GC electrodes show significantly improved catalytic activity. The electrochemically activated Au/GC electrode shows better catalytic properties than the freshly prepared one. Therefore, only the results on modified electrodes obtained after 30 cycles will be presented further in this work. Figure 3b shows the polarization curves for ORR on the electrodes obtained after Au electrodeposition for 5, 10, and 30 minutes on GC and Au(poly) for

comparison. The initial potential for the ORR on Au(poly) is approx. 0.2 V. It is higher for all examined Au/GC electrodes: 0.3 V for 5minAu/GC and 10minAu/GC electrodes and approx. 0.4 V on 30minAu/GC electrode. For the most active 30minAu/GC electrode, the initial potential for ORR is shifted positively for 200 mV compared to Au(poly).

3.3. Electrochemical behavior of PdAu/GC electrodes

Figure 4 illustrates the electrochemical behavior of PdAu/GC electrodes obtained by spontaneous deposition of palladium for 3 and 30 minutes on previously prepared 30minAu/GC substrates. CVs in Figure 4a are recorded first in potential range from -0.2 V to 0.9 V, where only oxidation/reduction of Pd occurs, and before the oxidation of gold begins. After a gradual opening of the positive potential limit to follow the oxidation/reduction of both Pd and Au, the CVs with the highest positive potential limit of 1.25 V are presented. CV of a bare GC electrode is also shown in the same wider potential region. At lower potentials, the hydrogen adsorption/desorption processes are observed on both PdAu/GC surfaces, which also confirms the presence of palladium. Both hydrogen adsorption/desorption and Pd oxidation/reduction peaks become significantly more pronounced with the increase of the deposition time. For 3minPd30minAu/GC and 30minPd30minAu/GC electrodes, the oxidation of palladium begins at 0.57 V and 0.50 V, while the reduction peaks occur at 0.59 V and 0.56 V, respectively. The coverage of 30minAu/GC electrode with the deposited palladium nanoparticles is estimated from the ratio between the charge passed during hydrogen adsorption on PdAu/GC and bare Pd(poly) electrode (210 μC/cm^2 [35]). The obtained coverage values are 5.5 % and 26.7 %, for 3 and 30 minutes Pd deposition, respectively.

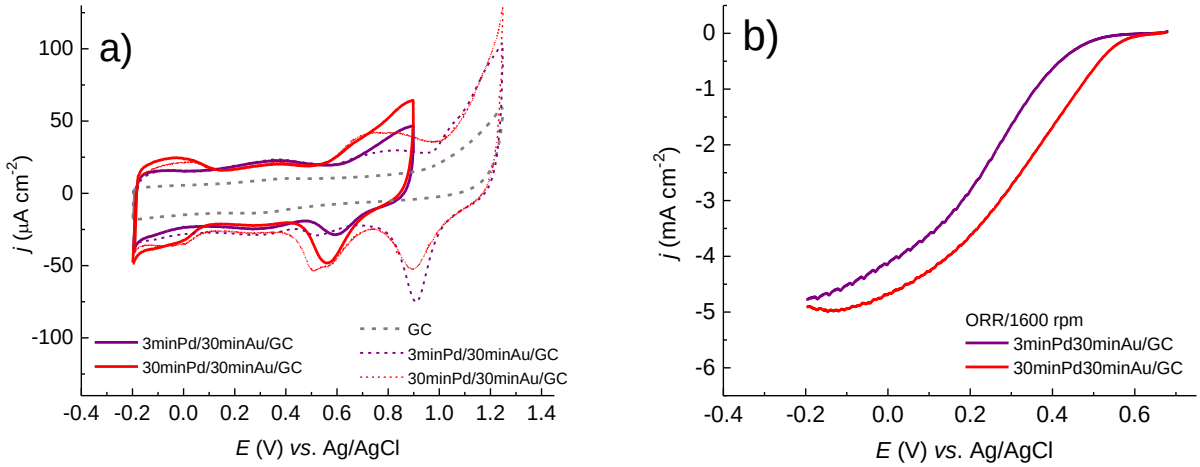

Figure 4. Electrochemical behavior of PdAu/GC electrodes obtained with Pd deposition times of 3 and 30 minutes: a) cyclic voltammograms recorded in deaerated 0.1 M $HClO_4$ solution; b) polarization curves for ORR recorded at 1600 rpm in 0.1 M $HClO_4$ solution saturated with oxygen. The scan rate was 50 mV/s.

The opening of the positive potential limit enables to follow the oxidation and reduction of both palladium and gold, with the highest potential set to 1.25 V before the beginning of the oxygen evolution reaction. CVs show two separate reduction peaks resulting from the reduction of palladium oxide at the potential of approx. 0.57 V and the reduction of gold oxide at 0.91 V. A decrease in the current density for palladium oxidation/reduction and hydrogen adsorption/desorption peaks for the upper limit of 1.25 V indicates a partial palladium dissolution at higher potentials [36].

Polarization curves for ORR on PdAu/GC electrodes obtained after spontaneous Pd deposition for 3 and 30 minutes on 30minAu/GC substrate electrode, Figure 4b, demonstrate a significant catalytic effect for oxygen reduction. The initial potential for ORR shifts to more positive values with increasing palladium coverage. For 3 min Pd deposition, ORR begins at ca. 0.55 mV, while for 30 min Pd deposition, it begins at approx. 0.65 mV. The comparative analysis of CVs in Figure 4a, and the initial potentials for ORR on the two PdAu/GC electrodes gives an insight the state of their surfaces. The initial potential for ORR on 3minPd/30minAu/GC falls in the potential region where the deposited palladium is metallic. On the other hand, on 30minPd/30minAu/GC ORR begins at the potential of partial palladium oxidation. In both cases, gold in PdAu nanoparticles stays metallic during ORR.

3.4. Comparison of the catalytic activity for ORR of the most active Au/GC and PdAu/GC electrodes

For comparison, Figure 5a shows LSV curves for bare GC, Au(poly), 30minAu/GC, 30minPd30minAu/GC, and Pd(poly). Compared to 30minAu/GC electrode, where ORR begins at 0.4 V, on 30minPd30minAu/GC the ORR begins at 0.65 V which coincides with the value obtained for the bare Pd(poly) electrode in 0.1 M $HClO_4$ solution [37]. The positive shift of the initial potential for 250 mV indicates a significant catalytic effect caused by the addition of Pd to Au/GC for oxygen reduction.

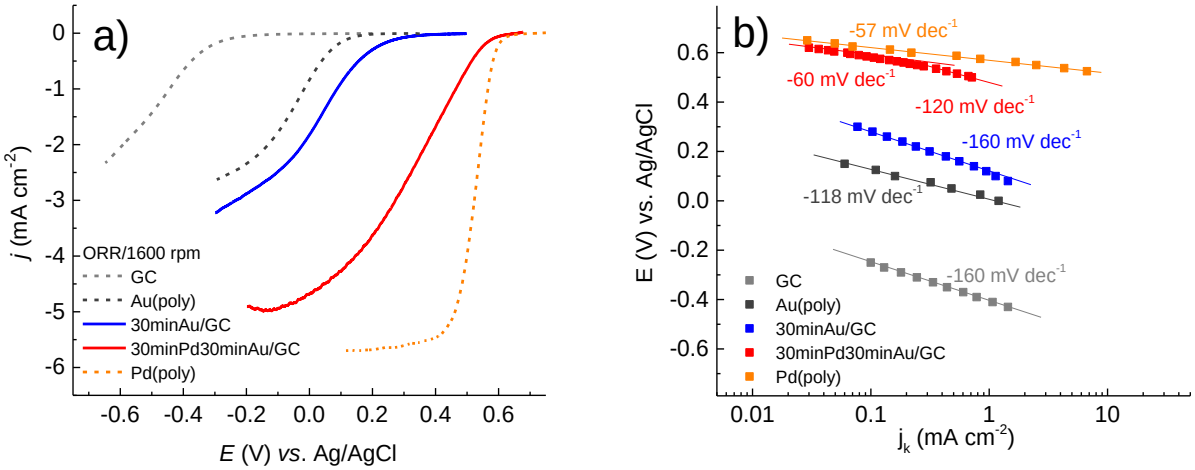

Figure 5. ORR on bare GC, Au(poly), Pd(poly), 30minAu/GC and 30minPd30minAu/GC electrodes: a) polarization curves recorded at 1600 rpm in 0.1 M $HClO_4$ solution saturated with oxygen. The scan rate was 50 mV/s; b) corresponding Tafel plots.

Figure 5b gives corresponding Tafel plots. Since the GC is a poor catalyst for ORR, with a slow reaction rate, the obtained higher Tafel slope of -160 mV/dec is suited. The same Tafel slope obtained for 30minAu/GC electrode is attributed to the influence of the GC substrate since for bare Au(poly) it is -118 mV/dec. Although based on the initial potentials, the activity of this electrode is much improved compared to Au(poly), the value of the slope indicates that the reaction rate is still slow. With the addition of Pd by deposition on Au/GC surface, the slopes become smaller. That means that the reaction rate increases at PdAu/GC electrodes. Two Tafel slopes for the 30minPd/30minAu/GC electrode are observed, following the change of the palladium oxidation state with potential. Namely, the oxygen reduction begins at a potential where palladium is partially oxidized and proceeds at more negative potentials, with the simultaneous Pd oxide reduction to the metallic state. Therefore, the slope of - 60 mV/dec corresponds to higher and - 120 mV/dec to lower potentials. These values are in agreement with the results obtained on various palladium-based catalysts, from bulk Pd [37,38] to Pd nanoparticles supported on gold [19] or carbon substrates [39,40]. Both Tafel slopes indicate that the rate-determining step is the exchange of the first electron. Therefore, although the mechanism for ORR might be the same, the kinetics depends on the surface state. The meaning of the Tafel slope concerning different surface state factors, as well as the electrode potential influencing the ORR mechanism are analyzed in detail in ref. [41].

In addition, Table 1 gives the results for ORR activity obtained in this work and similar PdAu nanostructures in acid solution.

Table 1. Comparison of the activity of different PdAu catalysts for ORR in acid solution

Catalyst	Solution	Rotation rate (rpm)	$E_{initial}$ (V)	$E_{1/2}$ (V)	Reference
30minPd30minAu/GC	0.1 M $HClO_4$	1600	0.65	0.31	This work
10 nm Pd thin film/Au(poly)	0.1 M $HClO_4$	1900	0.66	0.54	[19]
120minPd/Au(poly)	0.1 M $HClO_4$	1600	0.55	0.36	[20]
Pd submonolayer/5-layer Au nanoclusters	0.1 M H_2SO_4	1500	0.55	0.15	[21]
Porous Pd layer/Au NPs/C Au:Pd (1:0.61)	0.5 M H_2SO_4	1600	0.64	0.54	[22]
Pd_9Au nanowires	0.1 M $HClO_4$	1600	0.74	0.69	[23]
Core-shell Au@Pd NPs	0.1 M $HClO_4$	1600	0.70	0.51	[42]
Core-shell cuboctahedral AuPd/C; Au:Pd (16:84)	0.1 M $HClO_4$	1600	0.76	0.64	[43]
Pd(poly)	0.1 M $HClO_4$	1600	0.65	0.53	[37]

The advantage of PdAu/GC electrodes explored in this work is the ease of their preparation and stability of PdAu nanoparticles (see ref. [27]). Their activity for ORR in perchloric acid solution did not

reach that of AuPd nanowires [23], or core-shell nanoparticles [42,43], but it falls within the range of the other similar systems. Ease of preparation, stability, and high activity provide a solid basis for improvement. The addition of a third element or modification of the carbon substrate may be an easy way to enhance the catalytic activity of such PdAu systems for ORR in acid solution.

4. CONCLUSIONS

Au nanoparticles are deposited electrochemically on glassy-carbon with full coverage and activated by potential cycling. The activity of thus prepared Au/GC for ORR in perchloric acid solution exceeds polycrystalline Au. AFM image analysis shows that the size of Au nanoparticles ranged from 10-50 nm. With the addition of spontaneously deposited palladium, AFM images show that the resulting PdAu/GC electrode consists of PdAu nanoparticles with a size in the range from 25-75 nm and that Pd is deposited preferentially on the edges of Au nanoparticles. Such PdAu/GC electrode shows remarkably high activity for ORR coinciding with those of polycrystalline palladium.

ACKNOWLEDGEMENT
The authors would like to thank the Ministry of Education, Science and Technological Development of Republic of Serbia (Grant No: 451-03-9/2021-14/200026) for financial support.

References

1. M.R. Tarasevich, A. Sadkowski, E.D. Yeager, *Oxygen Electrochemistry,* in: B.E. Conway, J.O'M Bockris, E. Yeager, S.U.M. Khan and R.E. White (eds.), *Comprehensive Treatise of Electrochemistry*, vo1.7., Plenum Press, New York, 1983, p.301-398.
2. R.R.Adžić, S.Štrbac, *J. Serb. Chem. Soc.,* 52 (1987) 587.
3. R.R. Adžić, S. Štrbac, N. Anastasijević, *Mater. Chem. Phys.,* 22 (1989) 349.
4. C. Jeyabharathi, U. Hasse, P. Ahrens, F. Scholz, *J. Solid State Electrochem.,* 18 (2014) 3299.
5. I. Srejić, M. Smiljanić, Z. Rakočević, S. Štrbac, *Int. J. Electrochem. Sci.* 11 (2016) 10436.
6. P. Ahrens, M. Zander, U. Hasse, H. Wulff, C. Jeyabharathi, A. Kruth, F. Scholz, *ChemElectroChem,* 4 (2017) 1.
7. M.S. El-Deab, T. Ohsaka, *Electrochim. Acta,* 47 (2002) 4255.
8. M.S. El-Deab, T. Okajima, T. Ohsaka, *J. Electrochem. Soc.,* 150 (2003) A851.
9. M.S. El-Deab, *Electrochim. Acta,* 54 (2009) 3720.
10. W. Chen, S. Chen, *Angew. Chem. Int. Ed.,* 48 (2009) 4386.
11. T. Inasaki, S. Kobayashi, *Electrochim. Acta,* 54 (2009) 4893.
12. J.S. Jirkovsky, M. Halasa, D.J. Schiffrin, *Phys. Chem. Chem. Phys.,* 12 (2010) 8042.
13. Y. Lee, A. Loew, S. Sun, *Chem. Mater.,* 22 (2010) 755.
14. A.J. Wain, *Electrochim. Acta,* 92 (2013) 383.
15. G. Vázquez-Huerta, G. Ramos-Sánchez, A. Rodríguez-Castellanos, D. Meza-Calderón, R. Antano-López, O. Solorza-Feria, *J. Electroanal. Chem.,* 645 (2010) 3513.
16. J.H. Shim, J.Kim, C. Lee, Y. Lee, *J. Phys. Chem. C,* 115 (2011) 305.
17. S.Y. Rhieu, V. Reipa, *Am. J. Nanomater.,* 3 (2015) 15.
18. H. Naohara, S. Ye, K. Uosaki, *Electrochim. Acta,* 45 (2000) 3305.

19. A. Sarapuu, A. Kasikov, N. Wong, C.A. Lucas, G. Sedghi, R.J. Nichols, K. Tammeveski, *Electrochim. Acta,* 55 (2010) 6768.
20. I. Srejić, M. Smiljanić, B. Grgur, Z. Rakočević, S. Štrbac, *Electrochim. Acta,* 64 (2012) 140.
21. M. Harada, H. Noguchi, N. Zanetakis, S. Takakusagi, W. Song, K. Uosaki, *Sci. Technol. Adv. Mater.,* 12 (2011), 044606/1.
22. J.H. Shim, J.Kim, C. Lee, Y. Lee, *Chem. Mater.,* 23 (2011) 4694.
23. C. Koenigsmann, E. Sutter, T.A. Chiesa, R.R. Adzic, S.S. Wong, *Nano Lett.,* 12 (2012) 2013.
24. A. Cha, J.H. Shim, A. Jo, S.C. Lee, Y. Lee, C. Lee, *Electroanalysis,* 26 (2014) 723.
25. T. Wang, A. Chutia, D.J.L. Brett, P.R. Shearing, G. He, G. Chai, I.P. Parkin, *Energy Environ. Sci.*, 14 (2021) 2639.
26. L. Rakočević, S. Štrbac, I. Srejić, *Int. J. Hydrog. Energy*, 46 (2021) 9052.
27. I. Horcas, R. Fernandez, J.M. Gomez-Rodriguez, J. Colchero, J. Gomez-Herrero, A.M. Baro, *Rev. Sci. Instrum.,* 78 (2007) 013705.
28. H. Angerstein-Kozlowska, B.E.Conway, B. Barnett, J. Mozota, *J. Electroanal. Chem.,* 100 (1979) 417.
29. H.Angerstein-Kozlowska, B.E.Conway, A.Hamelin, L.Stoicoviciu, *Electrochim. Acta*, 31 (1986) 105.
30. S. Štrbac, R.R. Adžić, A. Hamelin, *J. Electroanal. Chem.,* 249 (1988) 291.
31. M.A. Schneeweiss, D.M. Kolb, D. Liu, D. Mandler, *Can. J. Chem.,* 75 (1997) 1703.
32. Y. Wang, Y. Sun, H. Liao, S. Sun, S. Li, J. W. Ager III, Z.J. Xu, *Electrochim. Acta*, 209 (2016) 440.
33. Y. Wang, E. Laborda, A. Crossley, R.G. Compton, *Phys. Chem. Chem. Phys.,* 15 (2013) 3133.
34. B.J. Plowman, N. Thompson, A.P. O'Mullane, *Gold Bulletin,* 47 (2014) 177.
35. M. Grden, M. Łukaszewski, G. Jerkiewicz, A. Czerwinski, *Electrochim. Acta,* 53 (2008) 7583.
36. E. Pizzutilo, S.J. Freakley, S. Cherevko, S. Venkatesan, G.J. Hutchings, C.H. Liebscher, G. Dehm, K. Mayrhofer, *ACS Catal.,* 7 (2017) 5699.
37. I. Srejić, Z. Rakočević, M. Nenadović, S. Štrbac, *Electrochim. Acta*, 169 (2015) 22.
38. L.M. Vračar, D.B. Šepa, A. Damjanović, *J. Electrochem. Soc.,* 133 (1986) 1835.
39. S.M. Senthil Kumar, J. Soler Herrero, S. Irusta, K. Scott, *J. Electroanal. Chem.,* 647 (2010) 211.
40. H. Erikson, A. Sarapuu, N. Alexeyeva, K. Tammeveski, J. Solla-Gulon, J.M. Feliu, *Electrochim. Acta,* 59 (2012) 329.
41. T. Shinagava, A.T. Garcia-Espanza, K. Takanabe, *Sci. Rep.,* 5 (2015) 13801.
42. D. Chen, C. Li, H. Liu, F. Ye, J. Yang, *Sci. Rep.,* 5 (2015) 11949.
43. A. Romero Hernández, M.E. Manríquez, A. Ezeta Mejia, E.M. Arce Estrada, *Electrocatalysis,* 9 (2018) 752.

© 2021 The Authors. Published by ESG (www.electrochemsci.org). This article is an open access article distributed under the terms and conditions of the Creative Commons Attribution license (http://creativecommons.org/licenses/by/4.0/).